J Mater Sci (2006) 41:5797–5801
DOI 10.1007/s10853-006-0140-6

LETTER

Sn–Sb–Se crystalline phases formed by melt-quenching technique

A. B. Adam · S. Sakrani · Y. Wahab

Received: 12 January 2005 / Accepted: 5 October 2005 / Published online: 13 May 2006
© Springer Science+Business Media, LLC 2006

Alloy percentages of Sn–Sb–Se (TAS) over a wide range of compositions were prepared, in specially designed shaking-furnace and melt-sealing evacuated quartz ampoule using the melt-quenching technique from 700 °C into liquid nitrogen. The characterization properties include structural, chemical compositions and surface morphology were obtained. XRD measurement was carried out to identify whether the as-prepared samples were amorphous or crystalline structure and to determine the boundary between the two states. It showed that Sn was incorporated in the ternary systems and formed crystal structure beyond 12.5-mol%. However, crystalline phases such as $Sn_2Sb_4Se_8$ and Sb_2Se_3 were mostly counted and dominant in crystalline structure samples with Sn-mol% more than 12.5. EDX was proved that the samples preserve their theoretical compositions and there was no excessive loss of either chalcogen or the additives. SEM morphological studies revealed that increasing Sn and Sb mole % modify the microstructure of the ternary Sn–Sb–Se-based systems. Under the same conditions of preparation and maintaining Sn mol% at 15, the dendrite-shapes of crystals were enlarged when Sb mol% increased.

Melt-Quenching technique (MQT) of preparing bulk glasses by means of rapid quenching of a melt is historically the most established and is still the most widely used in the preparation of amorphous chalcogenide materials [1]. Unusual behavior of Sn–Sb–Se alloys is the occurrence of wide range of crystalline structure using this method. It may be due to Sn and Sb heavy atomic masses [2], long atomic radius [3], high ionicity, low covalently, few number of lone-pairs [4, 5] and large amount of average co-ordination numbers, $\mu > 3$, with chalcogenide elements particularly Se [6–8]. Previous reports about Sn–Sb–Se (TAS) systems are shown in [9–16]. The aim of this paper is to report the characteristics of Sn–Sb–Se crystalline phases formed by MQT.

Granules of Sn and Sb having 99.999% purity while that of Se having 99.99% purity were used. The containers that these materials were stored in were only opened under controlled conditions to minimise contamination. Samples were batched in a closed scale balance on which Sn, Sb and Se were weighted in accurate 0.01 g using sample percentage procedures as mentioned in [10]. Batched elements were placed in the pre-cleaned quartz ampoule. The ampoule was attached to the vacuum pump and evacuated up to 0.5-mm Hg. Then an inert argon gas was applied for half an hour while the pumping continued. The ampoule was then sealed using an oxygen-natural gas flame melt, by heating its wall, bending it carefully and sealing it up. It was mentioned that selenium is recognised as high vapour pressure and tendency to react with oxygen. Thus, care and precaution were taken to avoid any explosion during the sealing process. Then, the ampoule was transferred into specially designed orbital-shaking furnace. Heating cycle up to 700 °C was applied at increasing rate of 5 °C per minute, followed by holding at this temperature for 6 h. The 700 °C was chosen according to previous studies [17–19] and also after many trials of three ranges of melting at 700, 800 and 900 °C. It seemed that, this melting temperature insured a complete melting of Sb and a minimum evaporation of Se. In order to prepare

A. B. Adam (✉)
Department of Electrical and Electronics Engineering, Universiti Teknologi PETRONAS, 31750 Tronoh, Perak, Malaysia
e-mail: abdallahbelal@petronas.com.my

S. Sakrani · Y. Wahab
Physics Department Faculty of Science, University Teknologi Malaysia, 81310 Skudai, Johor, Malaysia

homogenous samples, agitation of 100.0 rotations per minute (rpm) was applied using an attached orbital shaker. Quickly, the ampoule was dropped in liquid nitrogen for fast cooling requirement. XRD analyses were performed on fine powder of 66-as-prepared samples using Siemens-Diffractometer D-5000, with energy of 40 KV, current 30 mA, CuKα, Lambda, λ = 1.5418 Å and resolution of 0.04°/m in the range of 2° to 60°. EDX energy of 2.09 KeV in a rate of 10 electron volts per charge, eV/ch, was applied to obtain elemental compositions. SEM was used to show the surface morphology and the microstructure development for the as-prepared samples with 1,000 rates of magnifications.

Some examples of XRD analysed samples that showed crystalline structures are symbolised in Figs. 1, 2, and 3, while their Miller indices are tabulated in Table 1. XRD analyses, intensity (arbitrary unit) versus the 2θ (degree) on selected binary Sn–Se samples are shown in Fig. 1. Spectra of $Sn_{7.5}Se_{92.5}$, $Sn_{12.5}Se_{87.5}$ and $Sn_{14.3}Se_{85.7}$ compositions are discussed. There are only two-needle peaks (001) and (004) that assigned to $SnSe_2$ and SnSe-crystalline phases, respectively. At the bottom only $SnSe_2$ peak is observed while SnSe peak is occurred at the rest spectra of high Sn mol%. The results imply the formation of $SnSe_2$ of the stoichiometric composition $SnSe_2$ at Sn = 7.5-mol%. The occurrence of crystalline phase in this composition may be due to Sn large atomic radius and high ionicity with Se. In contrast, small addition of Sb mol% (2.5%) is sufficient to disturb the order of the bonds and enhance the glass formation as reported in [10]. Beyond this composition on Sn–Se binary line all samples were found completely in crystalline structures [10].

In Fig. 2, two peaks are observed in a bottom spectrum of $Sn_{15}Sb_5Se_{80}$. A peak with Miller index (001) corresponds to $SnSe_2$ crystalline phase, while that with a high

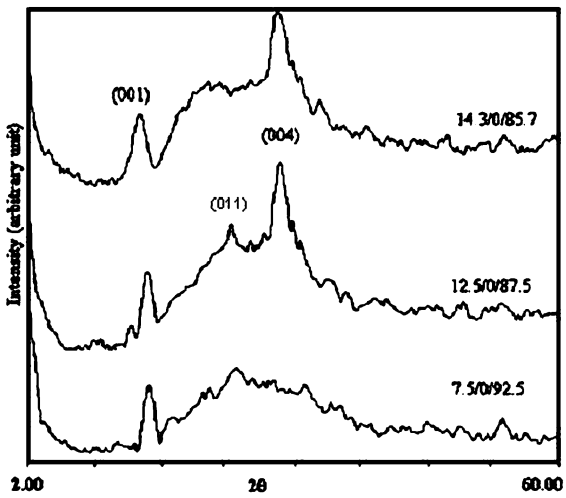

Fig. 1 XRD patterns of some selected samples of binary Sn–Se systems (Adam et al. submitted Letter Jan. 2005)

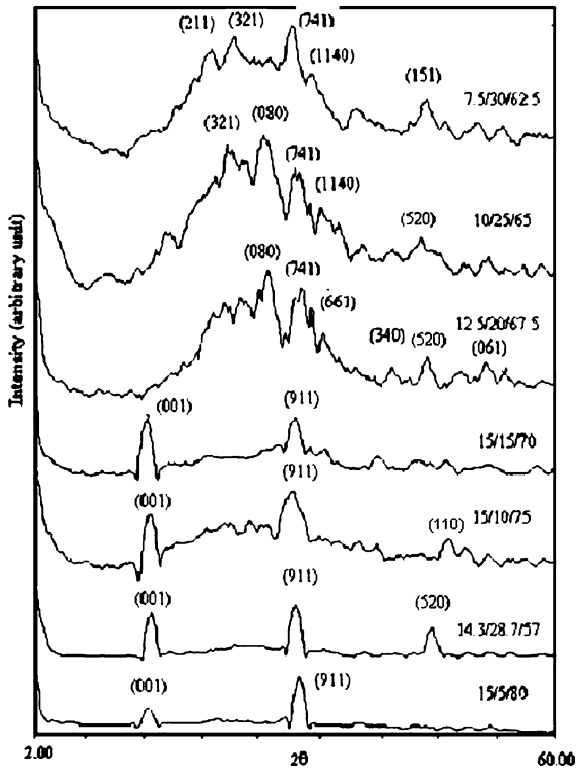

Fig. 2 XRD patterns of some selected samples of ternary Sn–Sb–Se systems (Adam et al. submitted Letter Jan. 2005)

intensity at (911) is for $Sn_2Sb_4Se_8$ crystalline phase. This later crystalline phase is dominant when its actual composition, $Sn_{14.3}Sb_{28.6}Se_{57.1}$, is prepared and analysed. Thus,

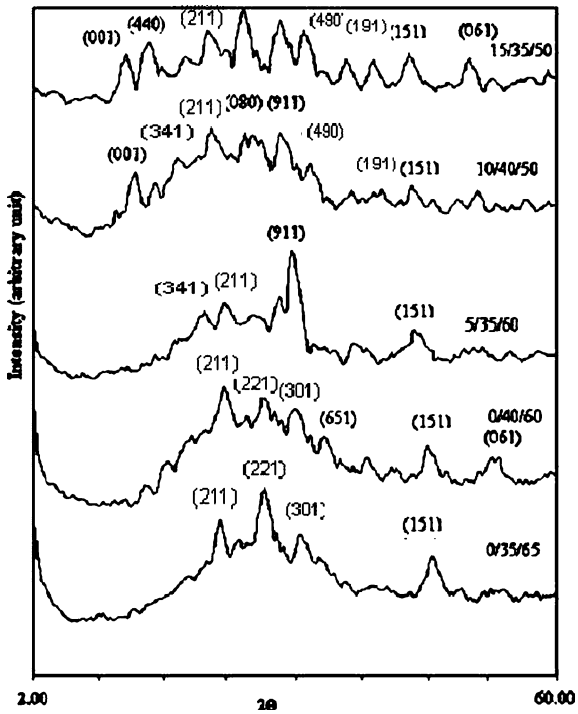

Fig. 3 XRD patterns of some selected samples of binary Sb–Se and ternary Sn–Sb–Se systems (Adam et al. submitted Letter Jan. 2005)

Table 1 XRD data for measured and standard Miller indexes of crystalline-phase samples (Adam et al. submitted Letter Jan. 2005)

Compound	Measured XRD			Standard		
	d_{khl} (Å)	I/I_0 (%)	*hkl*	d_{khl} (Å)	I/I_0 (%)	*hkl*
$SnSe_2$	6.14	83.84	001	6.14	9	001
SnSe	3.04	18	011	3.054	16	011
SnSe	2.88	100	004	2.87	50	004
$Sn_2Sb_4Se_8$	3.21	100	080	3.25	12	080
$Sn_2Sb_4Se_8$	2.869	82	741	2.874	100	741
$Sn_2Sb_4Se_8$	5.21	60.98	440	5.22	35	440
$Sn_2Sb_4Se_8$	3.33	10	341	3.345	6	920,341
$Sn_2Sb_4Se_8$	2.8213	100	911	2.831	57	911
$Sn_2Sb_4Se_8$	2.73	50	490	2.749	52	490
$Sn_4Sb_4Se_{10}$	2.8213	100	911	2.817	21	911
$Sn_4Sb_4Se_{10}$	3.74	80.0	920, 321	3.74	14	920, 321
$Sn_4Sb_4Se_{10}$	2.87	100	1140	2.871	100	1140
$Sn_4Sb_4Se_{10}$	2.36	27	191	2.362	23	191
Sb_2Se_3	5.21	60.98	440	5.25	55	120
Sb_2Se_3	3.20	100	211	3.23	60	211
Sb_2Se_3	2.88	100	004	2.868	100	221
Sb_2Se_3	2.76	34	301	2.776	60	301
Sb_2Se_3	2.17	50.86	520	2.164	20	520
Sb_2Se_3	2.09	20.65	440	2.076	10	440
Sb_2Se_3	2.652	71.35	661	2.661	20	661
Sb_2Se_3	2.341	44.68	340	2.345	14	340
Sb_2Se_3	1.995	57.29	151	1.998	25	151
Sb_2Se_3	1.761	42	061	1.761	45	061

$Sn_2Sb_4Se_8$ phase is observed in the second spectrum from the bottom. The lattice parameters, *a, b* and *c* of orthorhombic $Sn_2Sb_4Se_8$ are 35.22, 26.03 and 4.15 nm, respectively [20]. Other peaks of $SnSe_2$ and Sb_2Se_3 are identified at (001) and (520), respectively. However, the peaks of those phases with addition peak at (110) which assigned to Sb_2Se_3-phase, are occurred in the rest spectra of $Sn_{15}Sb_{10}Se_{75}$ and $Sn_{15}Sb_{15}Se_{70}$. It is worth mentioning that Sn–Se bond clearly dominant in the spectra that have compositions of Sb less than 15-mol%. Needle shape peak (001) of $SnSe_2$ is completely disappeared when the spectrum of $Sn_{12.5}Sb_{20}Se_{67.5}$ is discussed as shown in Fig. 2. However, many peaks of Sb_2Se_3 crystalline phase are identified at (520), (211), (061) (340) and (661) and implied the preference of this phase. Peaks at (080) and (741) are ascribed to $Sn_2Sb_4Se_8$ crystalline phase, wile that at (321) is assigned to $Sn_4Sb_4Se_{10}$-phase. These three crystalline phases are counted in the rest of the spectra of $Sn_{10}Sb_{25}Se_{65}$ and $Sn_{7.5}Sb_{30}Se_{62.5}$ samples. The lattice parameters, *a, b* and *c* of orthorhombic $Sn_4Sb_4Se_{10}$ are 35.16, 25.96 and 4.14 nm, respectively [20].

Figure 3 shows XRD spectra of samples that have average co-ordination number $\mu \leq 2.4$ and fraction of Sn–Se bond less than 44.5%, which were assumed theoretically to be in amorphous state [9]. As shown in this Figure, the bottom spectrum demonstrates $Sb_{35}Se_{65}$ sample with many peaks at (211), (221), (301) and (151), which assigned to Sb_2Se_3 crystalline phase. However, the same peaks are observed in stoichiometric composition $Sb_{40}Se_{60}$ with another additional peaks at (651) and (061). These crystalline phases are in agreement with that reported in [2, 21]. Increasing Sb-mol% above 30 provides extra cations that enhance the crystalline structure of the samples, while Sb-coordination number with Se is increased from 3 to 5 resulting in Se-coordination number to be 3 instead of 2. Addition of Sn-mol% to those samples in this rich area of Sb-mol% increases the formation of ternary crystalline phases due to the donations of more cations. As shown in Fig. 3, new crystalline peaks are occurred at (341) and (911) and assigned to Sn_2Sb_4Seg or $Sn_4Sb_4Se_{l0}$ in sample $Sn_5S_{35}Se_{60}$. The additions peaks at (211) and (151) are attributed to Sb_2Se_3 crystalline phase. Similar peaks are observed in the spectra of $Sn_{10}S_{40}Se_{50}$ and $Sn_{15}S_{35}Se_{50}$ samples. On other hand, $SnSe_2$ crystalline phase is appeared at (001) while the peaks at (080), (490) and (191) are assigned for Sn_2S_4Seg or $Sn_4S_4Se_{10}$ crystalline phases.

XRD results shown in Figs. 1, 2 and 3 can be explained in accordance with the report of [22] on X-ray studies of two compositions $Sn_2S_4Se_8$ and $Sn_4S_4Se_{10}$ in the SnSe–Sb_2Se_3 system. As stated earlier, SnSe has a deformed NaCl-type structure with each atom co-ordinates in the form of a strongly distorted octahedron. For Sb_2Se_3 chains of –Sb–Se–Sb oriented along the *c*-axis build up the structure. In both cases, the chain structure of Sb_2Se_3 is most probably the dominant structure-building factor. Their explanation is capable of clarifying the crystalline

structure of Sn–Sb–Se systems in this region. Influence of replacement of Ge by Sn on glass formation and physico-chemical properties of glasses in the Sb–Ge–Se system was reported [23]. They stated that Sn does not form glasses with Se. He found that the glass formation of the Sn–Se system was much more difficult than that of Ge–Se system. It was mainly ascribed to the ionicity difference between Ge–Se and Sn–Se in the chemical bond, which gives a large influence on the glass forming ability and vibration properties. The ionicities of Ge–Se and Sn–Se bonds are 0.21 and 0.48 atomic units (a. u.), respectively.

Table 2 shows EDX result for selected samples. It illustrates that all three elements are involved in each components of ternary samples with minor deviation from the nominated one, which was neglected. It is worthy to mention that from EDX analysis no impurity was detected, which may be due to the fact that, EDX does not detect elements if their weight % are very low. However, the results imply that no material was lost during the preparation. Accordingly, the nominal percentage was considered as the actual measured one and used for describing all samples in this study.

Figure 4 shows the surface morphology and the microstructure development of as-prepared samples with 1,000-magnifications of ternary Sn_{15}–Sb_x Se_{85-x} systems, where x = 5, 10, 15 and 20 of Sb-mol%, respectively. The surface's feature of the top image of Sb = 5-mol% shows distinguishable cloud shapes, while unclear grain boundaries among them are observed imply the crystalline structure of the sample. The occurrence of these crystallites probably related to the existing of Sn and Sb mol%. These can be understood in the fraction of the bond calculation in [10] showed the fraction of Sn–Se is 51.1%, while that of Sb–Se and Se–Se bonds are 12.8% and 36.2 %, respectively. Therefore, these white colour crystallite shapes properly consist of $SnSe_2$ and $Sn_2Sb_4Se_8$ crystalline phases as shown in Fig. 2. The surface morphology is changed and shoed a new crystallite features of Sb-mol% = 10 image. Crystallites, with distinguishable grain boundaries, agglomerate together and show spherule-shapes among dendrite forms, which imply the dispersing ability of Sb in Se. This dispersing ability can also be correlated to the ionicity, bond energy and co-ordination number of the bond that increases the fraction of the Sb–Se bonds than that of a previous sample. The ionicity of Sb–Se bonds is 0.34 a. u., which less than that of Sn–Se [4]. The surface morphology is completely modified and spherule-shapes among the dendrite forms are observed, when image of Sb = 15-mol% is examined. Grains with diameters of 20 μm and less are appeared, which indicate the formation of $SnSe_2$ and Sn_ZSb_4Seg crystalline phases. These findings can be supported by the fraction of the bond and average co-ordination number that calculated in [10]. Fraction of Sn–Se is 49.0%, which is more than 44.5% that was assigned for crystalline phase $Sn_ZSb_4Se_8$. Secondly, XRD analysis on this sample showed crystalline peak of this phase, while glass transition temperature is disappeared [10]. Finally, the average co-ordination number of this sample is 2.5, which is more than 2.4 the average co-ordination number of crystalline phase Sb_2 Se_3. Similar change of surface morphology is observed when image of Sb = 20-mol% is exposed. Grains with diameters of 20 μm and less are identified, which indicate the formation of many Sb_2Se_3 crystalline phases in addition to $SnSe_2$ and Sn_ZSb_4Seg phases. The fraction of Sn–Se and Sb–Se bonds of this sample is 48.0%. It is for Sn–Se is more than 44.5% that was assumed theoretically and found experimentally in $Sn_2Sb_4Se_8$ crystalline phase. The f_{Se-Se} bond is equal to 4.0% [10]. Finally, its average co-ordination number, μ = 2.5, which is more than 2.4 the average co-ordination number of crystalline phase Sb_2Se_3.

From the above-results it is concluded that. $Sn_2Sb_4Se_8$ is the most commonly encountered crystalline phases. It occurred along the Sn mol% = 15 in ternary compositions and supports the theoretical argument that considered Sn mol% = 14.3 is the boundary line between crystalline and

Table 2 Theoretical (T) and measured (M) weight percent of representative samples of Sn–Sb–Se that analysed using EDX probe

Elements	Sn (Wt. %)		Sb (Wt. %)		Se (Wt. %)	
Sample	T	M	T	M	T	M
15/5/80	20.23	22.14	7.01	6.80	72.76	71.06
20/5/75	27.34	26.80	7.00	7.13	65.66	66.07
25/5/70	33.47	34.21	6.98	6.56	59.55	59.23
15/10/75	19.96	21.13	13.7	15.03	66.4	63.84
20/10/70	26.0	26.74	13.4	14.75	60.6	58.51
25/10/65	37.4	37.49	12.8	13.48	49.8	48.03
15/15/70	19.20	20.61	20.23	20.25	60.57	59.14
20/15/65	24.95	25.54	20.01	21.32	55.05	54.14
30/15/55	37.14	38.42	19.43	20.12	44.43	41.46
20/20/60	24.68	24.25	26.65	27.53	48.67	48.22
30/20/50	36.01	37.54	24.38	25.41	39.61	37.05

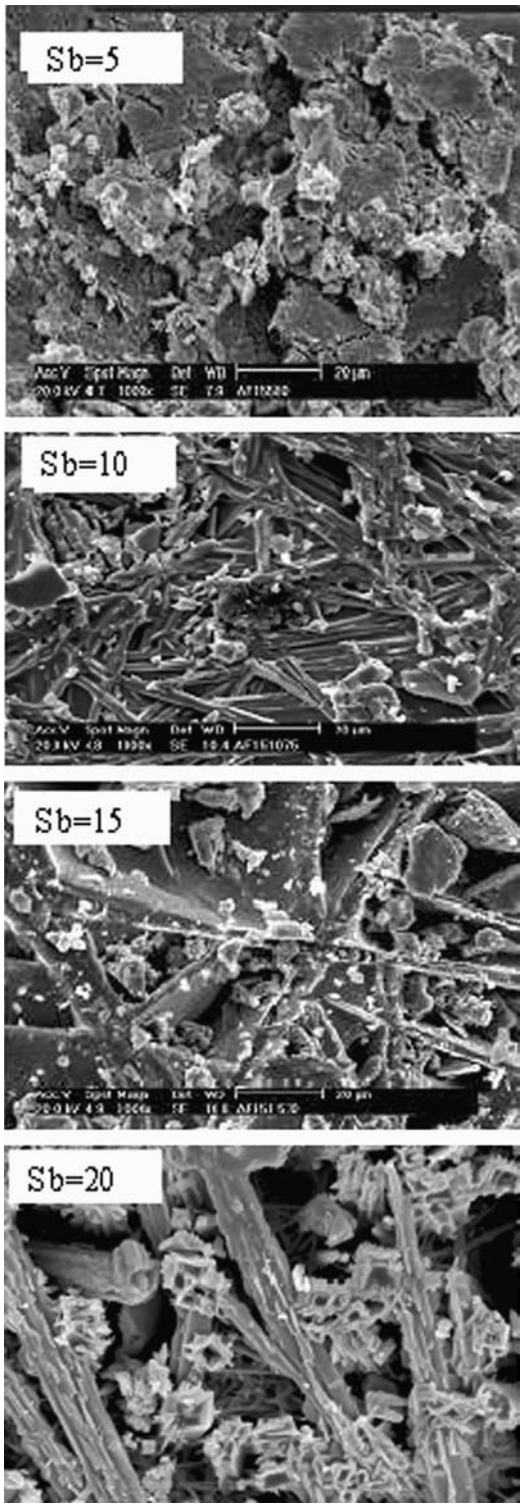

Fig. 4 SEM images on $Sn_{15}Sb_xSe_{85-x}$ where x = Sb-% = 5, 10, 15 and 20 (Adam et al. submitted Letter Jan. 2005)

amorphous region. Other crystalline phases such as Sb_2Se_3, $SnSe_2$, SnSe and $Sn_4Sb_4Se_{10}$ were found in the tie binary lines and ternary compositions. On the other hand, Sb_2Se_3 crystalline phase is dominant in the region with Sb-mol% more than or equal to 15. SEM morphological studies revealed that increasing Sn and Sb mol% modify the microstructure of the ternary Sn–Sb–Se-based systems. However, there are remarkable influences on the morphology of the crystal growth when large amounts of Sn and Sb are added. Under the same conditions of preparation, the dendrite-shapes of crystals are increased by increasing Sb mol% when Sn mol% is maintained at 15. Finally, MQT proved its ability in preparing alloy of Sn–Sb–Se in crystalline structure and there was no excessive loss of the materials during the preparation.

Acknowledgement The corresponded author was grateful to University of Kordofan, Sudan and University of Technology, Malaysia for their financial support.

References

1. Elliott SR (1991) In: Zarzychi JW (ed) Glasses and amorphous materials, vol 9. New York, VCH
2. Hilton AR, Jones CE, Brau M (1966a) Phys Chem Glasses 7(4):105
3. Chelikowsky JR, Philips JC (1978) Phys Rev B 17(6):2453
4. Zhenhua L (1991) J. Non-Cryst Solids 127:298
5. Fouad SS, Fayek SA, Ali MH (1998) Vacuum 49:25
6. Philips JC (1979) J Non-Cryst Solids 34:153
7. Lezal D (2003) J Optoelectron Adva Mater 5(1):23
8. Elliott SR (1990) Physics of amorphous materials. Longman Scientific & Technical Press, New York
9. Adam AB, Sakrani S, Wahab Y (2005) J Mat Sci 40(7):1571
10. Adam AB (2002) PhD-Thesis. University of Technology, Malaysia
11. Adam AB, Sakrani S, Wahab Y (2004) Physical Characterizations of Sn_x–Sb_{15}–Se_{85-x} Chalcogenide Glasses. Paper submitted on Dec.7, 2004, to be published in Journal of Materials Science
12. Adam AB, Sakrani S, Wahab Y (2002) J. Solid State Sci Tech 10(1&2):139
13. Wahab Y, Adam AB, Sakrani S (2002) J Solid State Sci Tech 10(1&2):60
14. Adam AB, Sakrani S, Wahab Y (2000) J. Solid State Sci Tech 8(1&2):42
15. Adam AB, Sakrani S, Wahab Y (1998) J Solid State Sci Tech 6(1):78
16. Sakrani S, Adam AB, Wahab Y (1997) J Solid State Sci Tech 5(1):1
17. Das GC, Platakis NS, Bever MB (1974) J Non-Cryst Solids 15:30
18. Agnihotri AK, Kumar A, Nigam A (1988) J Non-Cryst Solids 101:127
19. Kakinuma F, Fukunaga T, Misawa M, Susuki K (1992) J Non-Cryst Solids 150:53
20. Mukherjee AK, Dhawan U, Kundra KD, Mondal M, Ali SZ (1982) Indian J Pure Appl Phys 20:681
21. Sreeram AN, Swiler DR, Varshneya AK (1991) J Non-Cryst Solids 127:287
22. Kislitskaya EA, Kokorina VF (1971) Translated from Zhurnal Prikladnoi Khimii 44(3):646
23. McNeil LE, Mikrut JM, Peters MJ (1987) Solid State Commun 62(2):101